Origin of “memory glass” effect in pressure-amorphized rare-earth molybdate single crystals.

Elena Willinger[1,2*], Vitaly Sinitsyn[1], Salavat Khasanov[1], Boris Redkin[1], Semeon Shmurak[1] and Eugeny Ponyatovsky[1]

[1]Institute of Solid State Physics, Russian Academy of Sciences, 142432, Chernogolovka, Russia.,
[2]Fritz-Haber Institute of the Max Planck Society, 14195, Berlin, Germany

E-mail: kudrenko@fhi-berlin.mpg.de

Abstract

The memory glass effect (MGE) describes the ability of some materials to recover the initial structure and crystallographic orientation after pressure-induced amorphization (PIA). In spite of numerous studies the nature and underlying mechanisms of this phenomenon are still not clear. Here we report investigations of MGE in β’-$Eu_2(MoO_4)_3$ single crystal samples subjected to high pressure amorphization. Using the XRD and TEM techniques we carried out detailed analysis of the structural state of high pressure treated single crystal samples as well as structural transformations due to subsequent annealing at atmospheric pressure. The structure of the sample has been found to be complex, mainly amorphous, however, the amorphous medium contains evenly distributed nanosize inclusions of a paracrystalline phase. The inclusions are highly correlated in orientation and act as “memory units” in the MGE.

1. Introduction.

The first observation of the MGE was reported for α-$AlPO_4$ (berlinite) [1]. The high pressure amorphization and recovery of the crystalline state on decompression was proven by *in situ* powder X-ray diffraction (XRD) and supported by infrared (IR) spectroscopy studies. Recovery of original optical birefringence of bulk single crystal samples after high pressure treatment was interpreted as evidence of the MGE: the compressed amorphous state had to retain “memory” of the initial

crystalline state and orientation. This work was followed by numerous experimental as well as theoretical studies of both pressure-induced amorphization (PIA) and closely related MGE in berlinite and other materials [2-10]. Some of them have raised doubts about the high pressure amorphization of $AlPO_4$ because transition from the α-phase to a poor crystalline phase was observed rather than transition to a purely amorphous state [10-11]. These observations brought one to argue that the MGE could in fact be a consequence of the memory effect associated with the underlying martensitic transformations [12]. An alternative suggestion was also considered on the physical nature of the MGE: the phenomenon was related to the rigid structural units, such as PO_4 in $AlPO_4$, in which the central atom (P) remains fourfold coordinated under pressure even when severely distorted [2-3]. In general it is implied that there should be "memory units" in PIA material for the MGE phenomenon to occur. However, such units have not been observed experimentally so far, and the MGE phenomenon is still of interest and widely discussed along with PIA. Rare-earth molybdates studied in this work show both irreversible PIA [13-14] and, probably, MGE upon subsequent annealing [15], and seem to be another model object, in addition to AlPO4, for investigation of the underlying mechanisms of the PIA-MGE phenomena.

Rare-earth molybdates, $RE_2(MoO_4)_3$ with RE = Pr, Nd, Sm, Eu, Gd, Tb, Dy or Ho, form an isostructural series. These compounds have two stable modifications at atmospheric pressure: a high-temperature β-phase (S.G.: $P\text{-}42_1m$) and a low-temperature α-phase (S.G.: $C2/c$). The difference in their crystal structures and specific volumes are rather large, $\Delta V/V \approx 25\ \%$[16]. By quenching, the high-temperature β-phase can be readily overcooled below $\beta \rightarrow \alpha$ transition temperature (around 1150 K, depending on the rare-earth cation) into the metastable β′-phase (S.G.: *Pba*2). The $\beta \rightarrow \beta'$ transition involves a small specific decrease in volume of about 0.5% (for temperatures of β′ below 450 K), again depending on the cation type[16].

The β′-phase crystals show a similar behavior under high pressure: they undergo phase transition at about 2.0GPa [19,21,22] and with further pressure increase gradually turn into the amorphous state which is irreversible at pressures of 9 GPa and higher [13-23]. Reverse transformation into the crystalline phase at ambient pressure takes place upon annealing at about 820 K [14,15,20]. The transformation results in a metastable β-phase rather than an α-phase, thermodynamically stable at these conditions, then on cooling the β-phase returns to the β′-phase[16]. Our recent studies have shown that the 2.0 GPa transition is of the martensitic type and reversible at

around 3.0GPa, in both polycrystalline and single crystalline samples, and the high pressure phase (HPP) corresponds to a novel phase of the $RE_2(MoO_4)_3$ molybdates [24].

In this work we took advantage of the irreversibility of the PIA under ambient conditions and carried out *ex situ* studies of the $RE_2(MoO_4)_3$ single-crystal samples subjected to PIA at 9 GPa as well as their subsequent structural transformations upon annealing at atmospheric pressure using the XRD and TEM techniques. Note that the rare-earth molybdates $RE_2(MoO_4)_3$ with RE=Sm, Eu, Gd or Tb show the same behavior upon PIA and annealing. Below we present the experimental data of more comprehensive studies on the $Eu_2(MoO_4)_3$ (EMO) crystal samples.

2. Experiment

The investigated single crystals of $Eu_2(MoO_4)_3$, $Gd_2(MoO_4)_3$ and $Sm_2(MoO_4)_3$ were grown from melt by the Czochralski method. The grown single crystals were of the orthorhombic β′-phase (Table 1). Then the crystals were cut to obtain rectangular parallelepipeds sized 3 x 3 x 1 mm^3 with (001), (110) and (1-10) facets. The high pressure treatment of the samples was performed in a toroid type high pressure chamber [25] under hydrostatic pressure of 9 GPa for 7 days at room temperature (hereinafter "treated samples"). The pressure-transmitting medium was either the 4 : 1 methanol – ethanol mixture or silicon oil. The values of pressure and treatment time were selected, first, because complete amorphization of the polycrystalline samples occurs at ~ 8.0-9.0 GPa, and second, because shorter treatment time of only 1 or 2 days leads to partial recovery of the β′-phase upon decompression. Completeness of the PIA of the samples was tested using optical spectroscopy [15]. The XRD studies were carried out using a CCD diffractometer (Oxford diffraction, Gemin-R) with Mo-radiation. The single crystal sample crystallographic orientations before and after PIA and the annealing processes were checked by the marks on the single crystal plate. Diffraction data were collected using small single crystal samples about 0.15 mm in size which were broken off from the bulk samples.

The single crystal plates for the TEM studies were 3 x 3 mm^2 x 40 μm in size and had (1-10) faceting. Thinning was performed by means of an argon-ion polishing system (Fishione 1010 Ion Mill) with a gun voltage of 4 kV at a liquid nitrogen temperature. The incident beam angle was set to 8^o in order to reduce radiation damage. Electron microscopy characterization of the samples was performed using a Jeol JEMS 100CXII transmission electron microscope operated at an accelerating voltage of 100 kV.

3. Results

The XRD data of the treated single crystal sample are shown in the Fig. 1. The integral two-dimensional (2D) X-ray diffraction pattern (Fig. 1A) was obtained by summarizing over all the X-ray oscillation diffraction patterns taken by rotation of the sample around three axes. It comprises the diffuse scattering rings as well as sharp peaks. The intensive diffuse scattering indicates that the sample has an amorphous-like structure while the sharp peaks are evidence of the presence of crystalline portions. Hence, one can conclude that the structure of the treated sample is complex and cannot be described by a purely amorphous state. Integration of the cumulative 2D diffraction pattern over the azimuthal angle results in a one-dimensional (1D) pattern (Fig. 1B). It exhibits three amorphous broad peaks with barely noticeable sharp diffraction maxima. The total intensity due to the crystalline diffraction peaks is much less than the integrated intensity of the halos. Quantitative analysis based on Debye patterns for the grinded samples showed that the degree of crystallinity varied from sample to sample and did not exceed 1-5%.

Further analysis of the diffraction patterns showed that all the observed sharp peaks can be attributed to the diffraction from the crystalline phase with an orthorhombic lattice, the parameters of which are listed in Table 1. The lattice parameters of the β′-phase and those of the high pressure phase (HPP) measured *in situ* at 2.3 GPa[24] are also listed in the table, for comparison. The first indicator of the HPP is the doubling of the c-parameter relative to the β′-phase, and this doubling is also observed in the crystalline phase of the treated sample. For the crystalline phase the reduced unit cell ($c_0 = c/2 = 9.70$ Å) volume ($V = 996$ Å^3) is by 15 % less than the unit cell volume of the β′-phase, which of the *in situ* HPP phase at 2.3GPa being less by 18%. The crystalline phase in the treated sample is indeed closely related to the HPP: not only the lattice parameters but also the observed diffraction intensities for both phases are in good agreement.

An important part of the observations is that the whole x-ray diffraction pattern of the crystalline constituent of the treated sample reveals a single crystal diffraction behavior: all the diffraction peaks are defined by a single reciprocal lattice matrix. This fact is illustrated by the reconstructed XRD [1-10] – zone pattern (Fig. 1C). As noted above, the indicator of the HPP is the doubling of the c- lattice parameter: the observed frequency of the reflections along the [001] direction corresponds to that

doubling. Thus it can be concluded that the minor crystalline content in the treated sample corresponds to the HPP phase (metastable at atmospheric pressure) and shows itself in diffraction as being a single crystal.

The next question is the morphology of the sample comprising both amorphous and crystalline constituents. To reveal the details of the microstructure of this complex solid, we carried out transmission electron microscopy studies.

Figure 1D shows a selected area of the electron diffraction (SAED) pattern of a sample area of about 0.5 μm. The SAED pattern also contains both single crystal diffraction spots and diffuse rings that again confirm the structural inhomogeneity of the sample. Comparison of the SAED pattern with the XRD [1-10]- zone pattern (Fig. 1C) shows that the observed single crystalline diffraction patterns are in good agreement and, hence, the SAED is produced by the crystalline constituent in the HPP state. Accordingly, the (004) reflection of the SAED was used to analyze the crystalline fraction content by dark field imaging. As shown in the Fig. 1E, the distribution of the bright contrast regions reveals that the crystalline component of the sample appears in the domains sized 30 nm or less, which are embedded in an amorphous matrix. These scattered inclusions, the nanosize islands in the amorphous medium, nevertheless produce a single crystalline diffraction pattern instead of a polycrystalline Debye pattern which means that the crystalline inclusions are highly correlated in orientation.

Thus the following model of the structural state of the “treated” EMO single crystal can be assumed. The structural state of the sample is inhomogeneous: the main part of the sample turns to a pressure induced amorphous structure. However, within this amorphous medium there are crystalline HP inclusions. The total HPP content does not exceed few percent. Although these inclusions are scattered in the amorphous matrix, they are highly correlated in their crystallographic orientation.

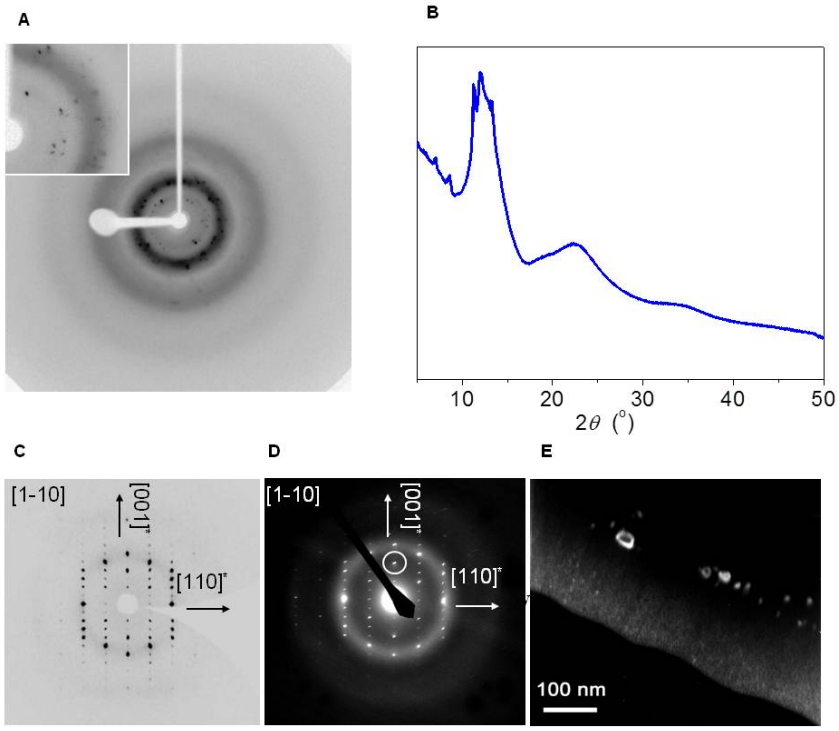

Figure 1. X-ray and electron diffraction from $Eu_2(MoO_4)_3$ crystal sample after high pressure (9 GPa) treatment: (a) cumulative X-ray diffraction pattern was obtained by summarizing all the oscillation diffraction patterns measured on CCD diffractometer. It comprises both the diffuse rings and sharp peaks (insert: enlarged central part; white shadow comes from beam-stop). Intensive diffuse scattering indicates that the sample has amorphous-like structure, while the sharp peaks are evidence of the presence of crystalline portions in the sample; (b) 1D reduction of the X-ray diffraction pattern demonstrates that the diffuse scattering consisting in three broad peaks over background is dominant, the total intensity due to crystalline sharp peaks corresponds to few percent of crystallinity; (c) crystalline part of the sample appears in diffraction as a single crystal of a high pressure phase (HPP): reciprocal space mapping (reconstruction of the X-ray oscillation patterns) in the (1-10) layer of HPP, observed frequency of the reflections along the [001] direction corresponds to the doubling of the ***c*** lattice parameter of HPP relative to that of β′-phase (see Table 1); (d) Selected area electron diffraction (SAED): every submicron part of the sample shows both diffuse scattering and HPP single crystal diffraction ([1-10]-zone axis pattern, (004) reflection is circled); (e) TEM dark-field image in

the (004) reflection: nanosize (≤30nm) bright domains are crystalline inclusions of HPP in amorphous sample, co-oriented to produce single crystal diffraction in the Figure 1d.

Table 1. Structural data of $Eu_2(MoO_4)_3$ single crystals at different treatment pressures

Phase, pressure	Crystal system	Space group	a, Å	b, Å	c, Å	V, Å^3	ΔV/V
β′-phase, atmospheric pressure	orthorhombic	*Pba2*	10.411(1)	10.444(1)	10.727(1)	1166.4(3)	0
HPP, 2.3GPa, *in situ*	orthorhombic	*Pca2$_1$*	9.470(1)	10.342(1)	19.511(2)	1910.9(6)	-18%
HPP, 9 GPa treated sample, *ex situ*	orthorhombic	*Pca2$_1$*	9.68(3)	10.61(4)	19.40(8)	1992(10)	-15%

The next step of our studies was to retrace the structural transformations in the treated samples under temperature annealing. Figure 2 presents the diffraction analysis data of the sample after annealing at 720 K for 3 hours.

Again, the sample is inhomogeneous as it is seen from the 2D integral diffraction pattern and its 1D transformation (Fig. 2A,B): it contains a dominating amorphous part with a crystalline contribution. But, as opposed to the case described above, the reconstructed XRD pattern (Fig. 2C) now demonstrates a single crystal diffraction pattern of the initial β′-phase: the diffraction spots corresponding to the doubling of the *c* parameters have disappeared (Fig. 2C) and the measured lattice parameters fit the β′-phase. The nanosize bright domains in the dark field image of the (002) reflection are correspondingly β′-phase crystalline inclusions in the amorphous medium (Fig.2E). The inclusions persist in their correlated orientation, for they produce single crystalline diffraction. Thus, the minor crystalline inclusions in the amorphous matrix undergo a correlated HPP→ β′-phase transformation due to annealing at 770 K, while the dominant amorphous matrix of the sample is preserved.

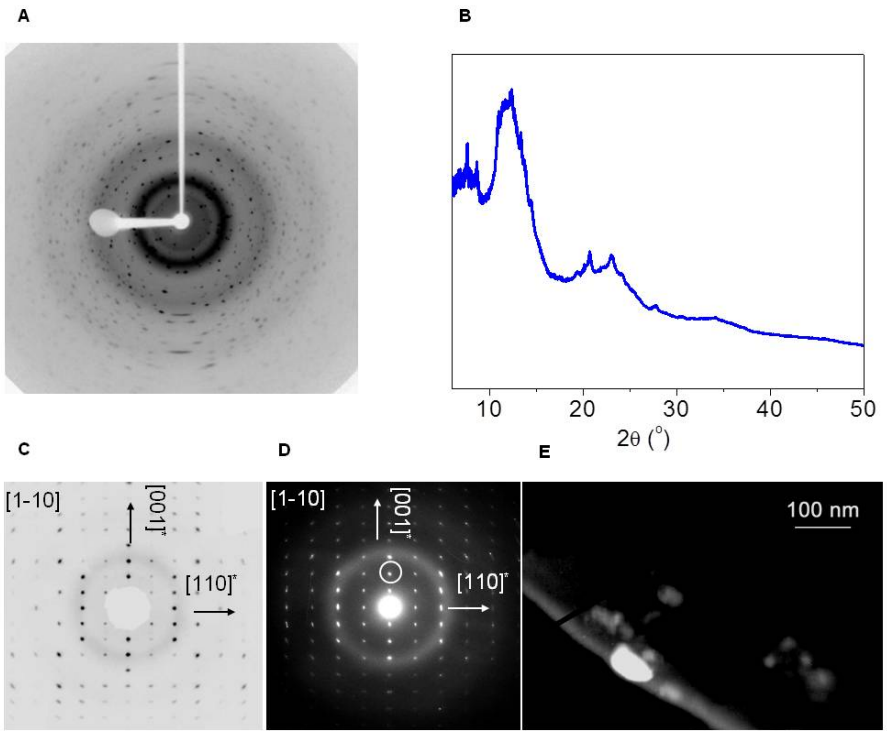

Figure 2. Diffraction analysis of the high pressure treated $Eu_2(MoO_4)_3$ crystal sample structure after annealing at 770 K: (a) cumulative X-ray diffraction 2D pattern shows both the diffuse rings and sharp peaks indicating two constituents in the sample, amorphous and crystalline; (b) 1D reduction of X-ray diffraction pattern demonstrates minority of the crystalline constituent; (c) crystalline part appears in diffraction as the β′-phase single crystal: reciprocal space mapping in the (1-10)-plane, doubling of the ***c*** lattice parameter, indicator of HPP, is absent; (d) SAED pattern: every submicron part of the sample shows both diffuse scattering and β′-phase single crystal diffraction ([1-10]-zone axis pattern, (002) reflection is circled); (e) TEM dark-field image in the (002) reflection: nanosize bright domains are crystalline inclusions of β′-phase in amorphous matrix, co-oriented to produce single crystal diffraction in the Figure 2d.

A drastic change in the diffraction pattern takes place after annealing at 820 K for 1 hour (Fig. 3). It is clearly seen that the 2D integral XRD pattern shows only diffraction spots and no signs of diffuse rings (Fig. 3A). The observed diffraction peaks correspond to the β′-phase single crystal diffraction (Fig. 3B). Hence, annealing at 820 K results in correlated transformation of the whole amorphous medium to the β′-phase single crystal state. The observed complete recovery of the

primary single crystalline state following severe distortion with a loss of long range order throughout sample clearly reflects an event of MGE.

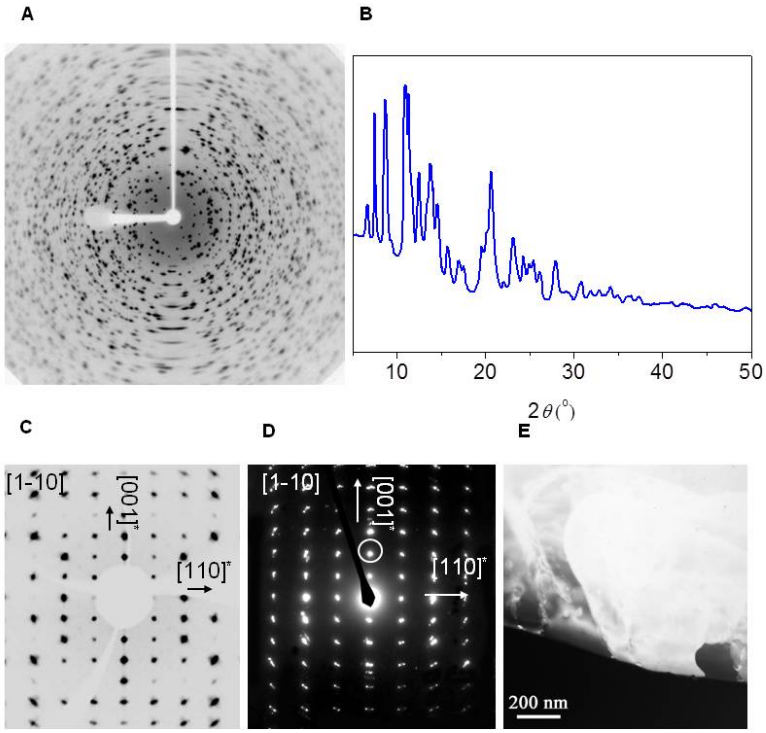

Figure 3. Diffraction analysis of the "treated" $Eu_2(MoO_4)_3$ sample structure after annealing at 820 K: (a) cumulative X-ray diffraction 2D pattern display only crystalline peaks; (b) 1D reduction of X-ray diffraction pattern reveal no amorphous constituent in the sample; (c) observed pattern corresponds to single crystal diffraction from β′-phase : reciprocal space mapping in the (1-10)-plane, doubling of the ***c*** lattice parameter, indicator of HPP, is absent; (d) SAED pattern along [1-10]-zone axis of β′-phase, (002) reflection is circled; (e), TEM dark-field image in the (002) reflection: bright domain is micron-size grain of β′-phase.

4. Discussion

As was mentioned above, the structural state of the treated sample mainly consists of an amorphous-like matrix that contains about 1-5% of residual crystalline inclusions from the HPP phase. These HPP inclusions measure around 30 nm and together, they produce a single crystalline

diffraction pattern. However, the diffraction pattern essentially differs from a common one: the reflections intensity degrades drastically with diffraction order. Figure S1 shows a comparison of the reconstructed X-ray diffraction patterns from residual crystalline nanodomains in the amorphous matrix of the HPP phase and the same nanodomains, but after back-transition to the β'-phase. One can see that in contrast to the β'-nanodomains showing regular higher order diffraction spots the HPP residuals produce a limited diffraction pattern. The diffraction spots are barely visible after the first diffuse ring and completely absent beyond the second diffuse ring of the amorphous state. This difference is an evidence of the frustrated order in the HPP nanodomains.

Furthermore, the one-dimensional HPP XRD pattern recorded along the (110)-direction of the sample displays significantly broadened diffraction orders (Fig. 2S). The broadening is clearly seen by comparing it with the one of the β'-phase recorded over the same 2Θ angle range. An estimation of the size of the coherently scattering regions by the Scherrer equation revealed 30 nm for the (220) and 15 nm for the (440), respectively. Both, the broadening behavior of the reflection orders and the loss of intensity at high orders prove that the crystalline state of the HPP is severely distorted.

All these observations indicate that the HPP structure in the inclusions can be described in terms of a paracrystalline state. The definition of a paracrystal was introduced by Hosemann et al. [26-27] as an intermediate state between the one of an ideal crystal and amorphous. It is classified as a state with distortions of a second kind, in which distortions lead to increasing of lattice point displacement with distance from the any origin ideal lattice point and at one moment getting more than the interplanar spacing. This has to be differentiated from distortions of the first kind, in which the average atomic positions over the crystalline lattice are preserved and the distortions have no influence on the long-range order of the lattice. Due to distortions of a second kind, the coherently scattered regions have limited sizes, and moreover, the size is scattering vector dependent. Indeed, coherent region boundary is determined as $\langle \Delta r \cdot S \rangle \sim 1$ where $\langle \Delta r \rangle$ is the total fluctuation of lattice planes, which is steadily increasing from the center towards higher plane numbers. Thus, the HPP nanodomains could be described as paracrystalline centers keeping some kind of an intermediate order throughout the amorphous matrix.

A similar phenomenon was observed for binary metallic and metalloid glasses obtained by the rapid quenching technique [28-29]. In contrast to the conventional model of the short-range order, for these glasses the concept of medium and extended topological order was introduced. Moreover, Zehng et al.

have shown that the high pressure devitrification of such an ordered glass results in formation of identically oriented crystallites of the face-centered cubic structure [30].

Another interesting example of structure memory effect is demonstrated in the organic bis(DL-serinium) oxalate dehydrate crystals [31]. The regular arrangement of molecular constituents in the crystal structure can be first distorted by compression and volume reduction, and then completely restored in a reversible manner on decompression. In this case, it is supposed that the strong hydrogen bonds in the structure preserve the main molecular network even in the pressure distorted structure and help in restoring the regular framework on decompression.

The pressure induced amorphization takes place in some tetrahedrally packed systems on a way of increasing pressure and goes through some polymorphic transformations. At one point the crystalline state gets unstable upon pressure but a next phase transformation is kinetically hindered. As a result the amorphization occurs [12]. This process can be followed in the Eu2(MoO4)3. The contraction at relatively low pressures results in the cooperative first order phase transition of a martensitic type from the β'-phase to the HPP phase. Further increase of the pressure leads to another structural transition with simultaneous progressive amorphization [19, 32]. One would expect that another phase transition would lead to the dense α-phase formation, which is the stable low temperature form of the molybdate. However, the transition is associated with significant structural rearrangements of the crystalline lattice since there is no subgroup relation between the HPP ($Pca2_1$) and the α-phase (C2/c). Additionally, the atomic diffusion is negligible at room temperature conditions and the system cannot overcome the energetic barrier for the structural transformation, a gradual amorphization occurs. At higher temperature, the high pressure induced transition to the α-phase would be expected.

Thus, summarizing the observations we can suggest the following mechanism of the MGE in rare-earth molybdates (Fig. 4). The initial β′-single crystal undergoes a martensitic transition to the HPP single crystal state under compression above 2.0 GPa (retaining the crystallographic orientation). The following increase in pressure leads to a partial amorphization of the sample and fragmentation of the HPP. After pressure treatment at 9 GPa the most part of the sample is amorphized except for few percent of its volume remaining in the HPP paracrystalline state. This small amount of the HPP is distributed over the sample as nanosized inclusions in the amorphous medium. Nevertheless, the HPP paracrystalline centers are highly correlated and keep the primary crystallographic orientation. Under annealing at moderate temperatures (below 770 K) these islands first transform from the paracrystalline HPP back to the parent crystalline β′-phase keeping the same crystallographic

orientation. Then the following annealing at higher temperatures induces growth of β′-phase islands by transforming the amorphous medium to the crystalline β′-phase. Finally, the initial crystalline state is restored.

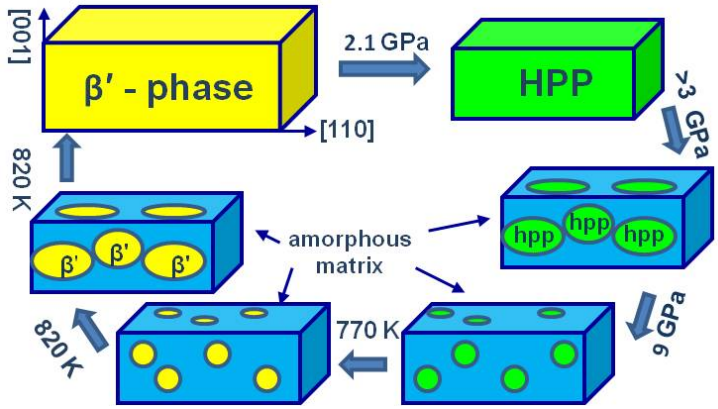

Figure 4. Schematic representation of PIA and MGE in rare-earth molybdate single crystals. Martensitic transformation from the β′-phase into the HPP takes place at 2.1 GPa. Further increase of pressure above 3GPa triggers amorphization and fragmentation of the HPP. After 9 GPa pressure treatment the sample state is mainly amorphous with a minor content of the paracrystalline HPP nanosize inclusions with the same crystallographic orientation. Reverse transformation occurs under annealing at 770 K resulting in the paracrystalline HPP→ crystalline β′-phase transition inside the inclusions. Annealing above 820 K leads to growth of the β′-phase islands by way of transition of the adjacent amorphous matrix to the β′-phase. Finally the original crystalline state is restored.

5. Conclusion

In conclusion, our observations convincingly demonstrate the origin of MGE in rare-earth molybdates to be result of presence of the residual paracrystalline nanodomains in the amorphous matrix. These identically oriented domains preserve the information about initial structure and orientation of the sample. They act as memory units and crystalline seeds during transformation of the amorphous phase back to the starting single crystalline β′-phase.

Acknowledgments

This work was supported by the Russian Foundation for Basic Research, Grant No. 12-02-00716, and by the Russian Academy of Sciences Research Program “The substances under high pressure compression”.

References

[1]. Kruger M B, Jeanloz R, 1990 *Science* **249,** 647

[2]. Tse John S, Klug Dennis D, 1992 *Science* **255,** 1559

[3]. Tse J S, Klug D D, Ripmeester J A, Desgreniers S, Lagarec K, 1994 *Nature* **369,** 724

[4]. Polian A, Grimsditch M, Philippot E, 1993 *Phys. Rev. Lett.* **71,** 3143

[5]. Gillet P, Badro J, Varrel B, McMillan R, 1995 *Phys. Rev. B* **51,** 11262

[6]. Sharma S M, Sikka S K, 1996 *Progr. Mater. Sci.* **40,** 1

[7]. Keskar N R, Chelikowsky J R, Wentzcovitch R M, 1994 *Phys. Rev. B* **50,** 9072

[8]. Watson G W, Parker S C, 1995 *Phys. Rev. B* **52,** 13306

[9]. Chaplot S L, Sikka S K, 1993 *Phys. Rev. B* **47,** 5710

[10]. Garg N, Sharma S M, 2000 *J. Phys.: Condens. Matter* **12,** 375

[11]. Sharma S M, Garg N, Sikka S K, 2000 *J.Phys.: Condens. Matter* ***12,*** *6683*

[12]. Bustingorry S, Jagla E A, 2005 *Physical Review B* **71,** 224119

[13]. Brixner L H, 1972 *Mater. Res. Bull.* **7,** 879

[14]. Ponyatovsky E G, Sinitsyn V V, Dilanyan R A, Red'kin B S, 1995 *JETP Letters* **61,** 222

[15]. Kiselev A P, *et al*., 2008 *Bull. RAS: Physics* **72,** 1297

[16]. Gschneider K A, 1979 *Handbook on the Physics and Chemistry of rare-earths(VI)* chap.30 *(North Holland Publisching Co., Amsterdam).*

[17]. Pal'nichenko AV, Ponyatovsky E G, Red'kin B S, Sinitsyn V V, 1998 *JETP Letters* **68,** 657

[18]. Jayaraman A, *et al.,* 1993 *J. Phys. Chem. Sol.* **54,** 827

[19]. Dmirtiev V, *et al*., 2003 *J. Phys. Chem. Sol.* **64,** 307

[20]. Kiselev A P, *et al*., 2006 *Phys. Sol. State* **48,** 1544

[21]. Machon D, Dmitriev V P, Sinitsyn V V, Lucazeau G, 2004 *Phys. Rev. B* **70,** 094117

[22]. Lucazeau G, Bouvier P, Pasturel A, Le Bacq O, Pagnier T, 2009 *Acta Phys. Pol. A* **116,** 25

[23]. Kudrenko E A, Shmytko I M, Sinitsyn V V, Ponyatovsky E G, Red'kin B N, 2008 *Z. Kristallogr.Suppl.* **27,** 205

[24]. Khasanov S S, *et al*., *Novel dense phase of the $RE_2(MoO_4)_3$ molybdates:crystal structure at 2.3GPa. (to be published)*

[25]. Khvostantsev L G, Slesarev V N, Brazhkin V V, 2004 *High pressure research* **24,** 371

[26]. Hosemann R, Baggi S, 1962 *Direct Analysis of Diffraction by Matter* (North Holland: Amsterdam 1962).

[27]. Balta Â-Callejaj F J, Hosemann R, 1980 *J. Appl. Cryst.* **13**, 521

[28]. Salmon P S, Martin R A, Mason P E, Cuello G J, 2005 *Nature* **435,** 75

[29]. Sheng H W, Luo W K, Alamgir F M, Bai J M, Ma E, 2006 *Nature* **439**, 419

[30]. Zeng Q, Sheng H, Ding Y, Wang L, Yang W, Jiang J-Z, Mao W L, Mao H-K, 2011 *Science* **332**, 1404

[31]. Zakharov Boris A., Boldyreva Elena V., 2014 *Journal of Molecular Structure* **1078**, 151-157

[32]. Le Bacq O, Machon D, Testemale T, Pasturel A, 2011 *Physical ReviewB* **83**, 214101